ORIGINAL ARTICLE

Line-field confocal optical coherence tomography for the in vivo real-time diagnosis of different stages of keratinocyte skin cancer: a preliminary study

C. Ruini,[1,2] (iD) S. Schuh,[3] C. Gust,[1] B. Kendziora,[1] (iD) L. Frommherz,[1] (iD) L.E. French,[1,4] D. Hartmann,[1] J. Welzel,[3,*,†] (iD), E.C. Sattler[1,†]

[1]Department of Dermatology and Allergy, University Hospital, LMU Munich, Germany
[2]PhD School in Clinical and Experimental Medicine, University of Modena and Reggio Emilia, Modena, Italy
[3]Department of Dermatology and Allergy, University Hospital, Augsburg, Germany
[4]Dr. Phillip Frost Department of Dermatology & Cutaneous Surgery, Miller School of Medicine, University of Miami, Coral Gables, FL, USA
*Correspondence: J. Welzel. E-mail: julia.welzel@uk-augsburg.de

Abstract

Background The treatment of keratinocyte cancers (KC) strictly depends on their differentiation and invasiveness. Non-invasive diagnostic techniques can support the diagnosis in real time, avoiding unnecessary biopsies. This study aimed to preliminarily define main imaging criteria and histological correlations of actinic keratosis (AK), Bowen's disease (BD) and squamous cell carcinoma (SCC) using the novel device line-field confocal optical coherence tomography (LC-OCT).

Methods Dermoscopy and LC-OCT images of 73 histopathologically confirmed lesions (46 AKs, 11 BD and 16 SCCs) were included in the study. Exemplary lesions (10 AKs, 5 BD and 5 SCCs) were additionally investigated with optical coherence tomography and reflectance confocal microscopy.

Results Most common LC-OCT findings of KC in the descriptive statistics were hyperkeratosis/parakeratosis, disruption of stratum corneum, broadened epidermis, basal and suprabasal keratinocyte atypia, dilated vessels/neoangiogenesis and elastosis/collagen alterations. In the univariate multinomial logistic regression, a preserved DEJ was less common in SCC compared with AK and BD, BD displayed marked keratinocyte atypia involving all epidermal layers (bowenoid pattern), while SCC showed ulceration, increased epidermal thickness, keratin plugs, acantholysis, not visible/interrupted DEJ and epidermal bright particles. LC-OCT increased the diagnostic confidence by 24.7% compared with dermoscopy alone.

Conclusions Our study describes for the first time specific LC-OCT features of different stages of KC and their histopathological correlates, focusing on keratinocyte morphology and architecture of the epidermis and DEJ. LC-OCT may open new scenarios in the bedside diagnosis, treatment planning and follow-up of KC.
Received: 19 February 2021; Accepted: 3 August 2021

Introduction

Keratinocyte skin cancer (KC), from its early stages of actinic keratosis (AK) and Bowen's disease (BD) to invasive squamous cell carcinoma (SCC), belongs to the most common tumours in elderly patients, related to chronic solar damage or immunosuppression.[1]

In order to prevent the transformation from subclinical keratinocyte dysplasia to invasive SCC and to lower the social and economic burden of the disease, early detection and treatment are essential.[2]

The diagnosis of KC is based on clinical and dermoscopical examination, eventually followed by a biopsy.[1] Dermoscopy has a good reported sensitivity and specificity in diagnosing and

---

[†]The authors share their senior authorship.
IRB approval status: Reviewed and approved by LMU Munich IRB; approval #17-699.

grading KC, although significantly higher for AKs (51.2%–98%; 95%) rather than SCCs (55%–79%; 84%–87%) and mainly calculated in the context of retrospective studies, so that further prospective studies are needed.[3–11] Non-invasive diagnostic methods such as reflectance confocal microscopy (RCM) and optical coherence tomography (OCT) have been widely used in the diagnosis of AKs[12–16], while few articles analysed the sensitivity and specificity of such tools for invasive SCCs.[14,17] RCM, which displays horizontal sections, allows a detection of characteristic AK patterns with high resolution[10,18]; however, its low penetration depth (up to 200–250 μm) can be a limit in evaluating the DEJ and the infiltration of the dermis in thick lesions. On the contrary, OCT does not permit a clear evaluation of cellular morphology in its vertical sections but is able to detect invasive lesions thanks to its higher penetration depth (up to 1.5 mm), and can display even their vascularity in dynamic mode.[19]

The new device line-field confocal OCT (LC-OCT) creates scans at higher resolution than conventional OCT, while reaching a higher detection depth compared to RCM, and can potentially be used for a non-invasive diagnosis of KC and several other skin diseases.[15,20–27] To date, no systematic studies on this topic have been published, so that we aimed to define main LC-OCT criteria for the diagnosis of KC, based on the histological criteria and the ones already described for similar diagnostic techniques. In addition, we preliminarily compared LC-OCT images with OCT and RCM to exemplarily point out the differences, strengths and limitations of the methods.

Materials and methods

Clinical, dermoscopic (FotoFinder GmbH, Germany and DermoGenius-DermoScan GmbH, Germany) and LC-OCT images of suspected KC were prospectively collected and analysed at the University of Munich and Augsburg. Cases were analysed by three imaging experts blinded to the histological diagnosis in a consensus, with an almost perfect agreement. In discordant cases, three more experts were involved for consensus. Only histopathologically confirmed lesions with a complete image set were included in the analysis. LC-OCT features were defined based on main histological parameters and the nomenclature chosen based on the current histology, OCT and RCM terminology. We chose not to define a novel terminology because LC-OCT allows a very intuitive comparison with the corresponding histological features because of its cellular resolution and visualization of vertical slices. Following criteria were investigated: epidermal thickness in μm (obtained with ten repeated measurements taken every 120 μm on the vertical image of the 1.2 mm long LC-OCT field of view in the centre of the lesion using the incorporated software tool), ulceration, disruption of stratum corneum (SC), hyperkeratosis, compact parakeratosis, scales, keratin plugs, thinning of the epidermis, broadened/acanthotic epidermis, suprabasal and basal atypical keratinocytes, bowenoid pattern, acantholysis, pyknotic cells, atypical honeycombed pattern, bright particles in the epidermis, dendritic cells, flattened rete ridges, well-defined dermo-epidermal junction (DEJ), not visible/interrupted DEJ, dilated vessels/neoangiogenesis, glomerular vessels, bright particles in the dermis and elastosis/collagen alterations. Keratinocytes were defined as atypical when visually markedly differing from each other in size, shape and contours compared with healthy skin. We defined the thickened, acanthotic epidermis with roundish ('bowenoid') contours built by enlarged atypical keratinocytes in all epidermal layers as 'bowenoid pattern'.

The level of diagnostic confidence was defined on a three-point scale from 0% to 100% as follows: high (>70%), average (51%–69%) and poor (<50%). LC-OCT images were acquired with a prototype device (DAMAE Medical, Paris), a class 1 supercontinuum laser with a central wavelength of 800 nm, with three imaging modalities: vertical and horizontal (1.2×0.5 mm^2) and 3D ($1.2 \times 0.5 \times 0.5$ mm^3). Instrument and acquisition procedures were described elsewhere.[21,28] Exemplary lesions (10 AKs, 5 BD and 5 SCCs) were imaged with a conventional OCT (VivoSight, Michelson-Diagnostics, UK) and RCM (VivaScope 1500–3000, Mavig, Germany) device.

Statistical analysis

For descriptive statistics, mean values with 95% confidence interval were calculated for numeric data, while absolute numbers with percentage portion were given for nominal data. To evaluate the discriminant value of LC-OCT features for the distinction between AK, BD and SCC, univariate multinomial logistic regressions were performed for each individual feature. Odds ratios (OR) with corresponding *P*-values representing the effect of one feature on the likelihood of a diagnosis being made were calculated for: (1) AK vs. BD and (2) BD vs. SCC (3) AK vs. SCC.

We additionally included all predictors that showed a significant OR in a multivariable multinomial logistic regression analysis, as done by Peppelman *et al.*[29] to estimate the correct classification rate that is reached by using all information contained in the predictors showing significance in the univariate multinomial logistic regression analyses. We excluded the results of this analysis from our results because of overfitting.

P-values of less than 0.05 were considered statistically significant. All statistical analyses were conducted using R (version 3.6.0, 2019, R Foundation for Statistical Computing).

All patients provided their written informed consent. The study was approved by the local ethics committee (No. 17-699).

Results

Population

123 lesions suspicious for KC were recruited prospectively of which 73 cases were enrolled after histopathologic confirmation (belonging to 25 females, 48 males, mean age 74.8 years, CI 72.7–76.9). Remaining cases were excluded due to missing histopathological confirmation of the diagnosis as gold standard. Forty-six

AKs (10 hypertrophic, 5 atrophic, 3 bowenoid), 11 BD and 16 invasive SCCs were analysed. Most common lesion site was the head and neck area (52.1% face, 28.8% scalp), followed by upper limbs (9.6%), lower limbs (5.5%), trunk (2.7%) and genital area (1.4%).

Diagnostic confidence
Our diagnostic confidence with LC-OCT was high in 74% and average in 26% of the cases; with dermoscopy, it was high in 49.3% and average in 49.3%. We therefore estimated an improvement of 24.7% compared with clinical examination and dermoscopy alone.

Morphological features
The descriptive statistics and the univariate multinomial logistic regressions of the dermoscopic features are available in Tables S1 and S2.

Main LC-OCT features of AKs in vertical mode as reported in the descriptive statistics were (Tables 1 and 2) (Figures 1 and 2, S1): hyperkeratosis with compact parakeratosis (95.7% and 67.1%, respectively), scales (67.4%), broadened acanthotic epidermis (68.2%) and keratinocyte atypia (95.5%). It was not always possible to exactly distinguish between basal and suprabasal layers. The DEJ was preserved in 82.6%. The dermis showed dilated vessels/neoangiogenesis (59.5%) and elastosis/collagen alterations (56.1%). BD was characterized by a marked keratinocyte atypia involving all epidermal layers (100%) but with a well-defined DEJ (80%) (Figures 1 and 3, S2). In 7 AKs and 2 BD, some parts of the DEJ were not visible.

In invasive SCC, hyperkeratosis (100%), ulceration (68.8%) and disruption of SC (100%), a marked keratinocyte atypia (100%) in a broadened epidermis (93.8%) was found, with an

Table 1 Descriptive statistics of LC-OCT features of actinic keratosis, Bowen's disease and squamous cell carcinoma evaluated in the study with their relative and absolute frequencies

Features	All subtypes		Actinic keratosis		Bowen's disease		Invasive squamous cell carcinoma	
	Mean	95% CI	Mean	95% CI	Mean	95% CI	Mean	95% CI
Epidermal thickness	155.8	134.0, 177.5	126.2	102.9, 149.5	168.5	107.1, 229.8	232.0	182.3, 281.7
	%	n	%	n	%	n	%	n
Epidermis								
Ulceration	23.9	17/71	6.8	3/44	27.3	3/11	68.8	11/16
Disruption of stratum corneum	82.2	60/73	71.7	33/46	100.0	11/11	100.0	16/16
Hyperkeratosis	97.3	71/73	95.7	44/46	100.0	11/11	100	16/16
Compact parakeratosis	83.6	61/73	67.1	35/46	100.0	11/11	93.8	15/16
Scales	78.1	57/73	67.4	31/46	90.9	10/11	100.0	16/16
Keratin plugs	50.7	37/73	39.1	18/46	54.5	6/11	81.2	13/16
Thinning of the epidermis	28.2	20/71	40.9	18/44	18.2	2/11	0.0	0/16
Broadened/acanthotic epidermis	78.9	56/71	68.2	30/44	100.0	11/11	93.8	15/16
Suprabasal atypical keratinocytes	71.2	52/73	54.3	25/46	100.0	11/11	100.0	16/16
Basal atypical keratinocytes	94.5	69/71	95.5	42/44	100.0	11/11	100.0	16/16
Bowenoid pattern	27.8	20/72	15.2	7/46	90.0	9/10	25.0	4/16
Acantholysis	23.2	16/69	15.9	7/44	20.0	2/10	46.7	7/15
Pyknotic cells	43.1	31/72	32.6	15/46	20.0	5/10	68.8	11/16
Atypical honeycombed pattern	97.2	70/72	95.7	44/46	100.0	10/10	100.0	16/16
Bright particles in the epidermis	31-4	22/70	25.0	11/44	10.0	1/10	62.5	10/16
Dendritic cells	5.7	4/70	4.5	2/44	20.0	2/10	0	0/16
Flattened rete ridges	56.5	39/69	65.1	28/43	5.5	6/11	33.3	5/15
Dermo-epidermal junction								
Well defined	68.1	49/72	82.6	38/46	80.0	8/10	18.8	3/16
Not visible/interrupted	28.8	21/73	15.2	7/46	36.4	4/11	81.2	13/16
Dermis								
Dilated vessels/neoangiogenesis	65.2	43/66	59.5	25/42	70.0	7/10	78.6	11/14
Glomerular vessels	13.6	9/66	9.5	4/42	20.0	2/10	21.4	3/14
Bright particles in the dermis	18.8	13/69	11.4	5/44	20.0	2/10	40.0	6/15
Elastosis/collagen alterations	61.9	39/63	56.1	23/41	70.0	7/10	75.0	9/12

CI, confidence interval; %, per cent (relative frequency); n, number (absolute frequency).

Table 2 Univariate multinomial logistic regression reporting odds ratios (OR) and *P*-values of main analysed LC-OCT parameters

Feature LC-OCT	Subtype	OR	P
Epidermal thickness	2|1	1.01	0.13
	3|1	1.01	*P* < 0.001***
	3|2	1.01	0.10
Ulceration	2|1	5.12	0.07050
	3|1	30.06	*P* < 0.001***
	3|2	5.87	*P* < 0.05*
Disruption of stratum corneum	2|1	5548.60	0.81
	3|1	9400.90	0.81
	3|2	15.70	0.98
Hyperkeratosis	2|1	978.45	0.88
	3|1	896.47	0.85
	3|2	12.36	0.98
Compact parakeratosis	2|1	2212.53	0.76
	3|1	4.72	0.15
	3|2	0.00	0.84
Scales	2|1	4.80	0.15
	3|1	8192.20	0.78
	3|2	1509.60	0.81
Keratin plugs	2|1	1.87	0.36
	3|1	6.74	*P* < 0.01**
	3|2	3.61	0.15
Thinning of the epidermis	2|1	0.32	0.18
	3|1	0.00	0.80
	3|2	0.00	0.85
Broadened/acanthotic epidermis	2|1	5689.80	0.80
	3|1	7.00	0.07
	3|2	0.00	0.99
Suprabasal atypical keratinocytes	2|1	12044.20	0.79
	3|1	20060.40	0.80
	3|2	12.60	0.99
Basal atypical keratinocytes	2|1	923.79	0.87
	3|1	867.28	0.84
	3|2	12.87	0.99
Bowenoid pattern	2|1	50.14	*P* < 0.001***
	3|1	1.86	0.38
	3|2	0.04	*P* < 0.05**
Acantholysis	2|1	1.32	0.75
	3|1	4.63	*P* < 0.05*
	3|2	3.50	0.18
Pyknotic cells	2|1	2.08	0.30
	3|1	4.55	*P* < 0.05*
	3|2	2.20	0.34
Atypical honeycombed pattern	2|1	1687.40	0.90
	3|1	3545.80	0.91
	3|2	12.4	0.98
Bright particles in the epidermis	2|1	0.33	0.32
	3|1	5.00	*P* < 0.01**
	3|2	15.00	*P* < 0.05*
Dendritic cells	2|1	5.250	0.12
	3|1	0.00	0.88
	3|2	0.00	0.84

Table 2 *Continued*

Feature LC-OCT	Subtype	OR	P
Flattened rete ridges	2|1	0.64	0.52
	3|1	0.27	*P* < 0.05*
	3|2	0.42	0.28
Well-defined DEJ	2|1	0.84	0.85
	3|1	0.049	*P* < 0.001***
	3|2	0.058	*P* < 0.01**
Not visible/interrupted DEJ	2|1	3.18	0.12
	3|1	9.28	*P* < 0.001***
	3|2	2.92	0.19
Dilated vessels/neoangiogenesis	2|1	1.59	0.54
	3|1	2.49	0.21
	3|2	1.57	0.63
Glomerular vessels	2|1	2.38	0.36
	3|1	2.59	0.26
	3|2	1.09	0.93
Bright particles in the dermis	2|1	1.95	0.47
	3|1	5.20	*P* < 0.05*
	3|2	2.67	0.30
Elastosis/collagen alterations	2|1	1.83	0.43
	3|1	2.35	0.25
	3|2	1.29	0.79

Nomenclature: 1 = actinic keratosis, 2 = Bowen disease, 3 = squamous cell carcinoma. Abbreviations: DEJ, dermo-epidermal junction; OR, odds ratio; Significance levels: **P* < 0.05, ***P* < 0.01, ****P* < 0.001.

either interrupted or non-visible DEJ (81.2%). (Figures 1 and 4). Dilated vessels/neoangiogenesis (78.6%) and collagen alterations (75%) were noticed.

In horizontal sections, SC was disrupted in 71.7% of AKs and 100% of SCCs; an atypical honeycombed pattern as described in RCM [13] was found in 95.7% of AKs and 100% of SCCs, pyknotic (broken) cells in 32.6% AKs, 68.8% SCCs. Collagen alterations and dilated vessels/neoangiogenesis were seen in all types of lesions; in 90% of BD, glomerular vessels (the typical tortuous, dilated vessels inside the dermal papillae) were displayed (Figure 3).

Mean epidermal thickness was 126.2 μm in AKs, 168.5 μm in BDs and 232 μm in SCCs (Table 1).

Univariate multinomial logistic regression models were performed to identify the main LC-OCT patterns allowing the distinction between different entities (AK, BD and SCC).[2] Following features were helpful in distinguishing SCCs compared to AKs: increased epidermal thickness (*P* < 0.001), ulceration (*P* < 0.001), keratin plugs (*P* < 0.001), acantholysis (*P* < 0.05), bright particles in the epidermis (*P* < 0.01), flattened rete ridges (*P* < 0.05), not visible/interrupted DEJ (*P* < 0.001) and bright particles in the dermis (*P* < 0.05). Ulceration (*P* < 0.05) and bright particles in the epidermis (*P* < 0.05) could analogously help differentiate a SCC from a BD, while the OR for BD well-defined DEJ (*P* < 0.01) and bowenoid pattern
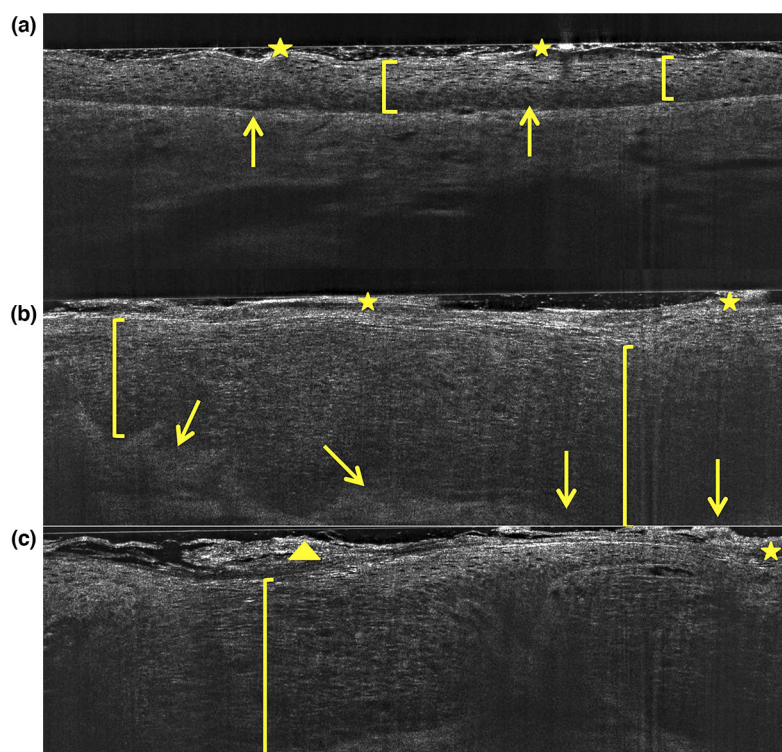
Figure 1 Different stages of keratinocyte skin cancer in LC-OCT, vertical mode: (a) AK of the face, (b) BD of the back, (c) SCC of the scalp. Hyperkeratosis and parakeratosis (star), atypical keratinocytes (bracket) are seen in all lesions; the DEJ (arrow) is preserved in (a) and (b), but not in (c), where strands of atypical keratinocytes infiltrating the dermis are seen (bracket) together with a thick, hyperkeratotic crust (triangle). AK, actinic keratosis; BD, Bowen disease; DEJ, dermo-epidermal junction; LC-OCT, line-field confocal optical coherence tomography; SCC, squamous cell carcinoma.

($P < 0.01$) was significantly higher for BD compared to SCC. The bowenoid pattern was the distinguishing feature of BD compared to AKs ($P < 0.001$).

Discussion

Differentiating stages of field cancerization noninvasively in real time is of outmost importance in the clinical practice since it allows an efficient therapy planning.

A dermoscopical 'progression model' was developed by Zalaudek *et al.*, who described a red pseudonetwork ('strawberry pattern') as typical for early AKs, and a red starburst pattern and yellow-white scales as a sign of transition to intraepidermal carcinoma. In BD, increasing neovascularization is seen as clustered glomerular vessels, while scales tend to become thicker and centrally coalesce. Advanced SCCs are characterized by irregular vessels, increased keratinization and ulceration.[3] Our findings were in line with the common literature on the topic: glomerular vessels were the most significant finding in dermoscopy of BD, while starburst pattern, scales and ulceration were seen in SCCs.

Conventional OCT, which provides vertical images intuitively comparable to histological sections and LC-OCT vertical mode, is able to detect common features of KC such as hyperkeratosis, epidermal disruption and loss of the DEJ. However, hyperkeratosis affects the imaging of underlying structures and an exact discrimination of the invasiveness is not always possible.[14,19,30–32] In their systematic review, Friis[19] described most common OCT features of AKs: disruption of layers, white streaks and dots and thickened epidermis. Schuh and Welzel demonstrated on a very large sample that AKs can be easily differentiated from normal skin and BCCs thanks to the decreased local signal intensity, as well as thicker SC and epidermis, finding moreover very good correlations between OCT and histopathological thickness of the skin layers.[33] In a paper focused on differentiation of non-melanoma skin cancers (NMSC), Batz *et al.* associated multifocal acanthosis to Bowen's disease and SCC, with SCC additionally showing hyperreflective nests and non-compressible dark borders.[34] No systematic study on OCT-guided diagnosis of SCC was published. Yet high-definition OCT (not commercially available anymore) was also used by Boone *et al.* for the in vivo discrimination of
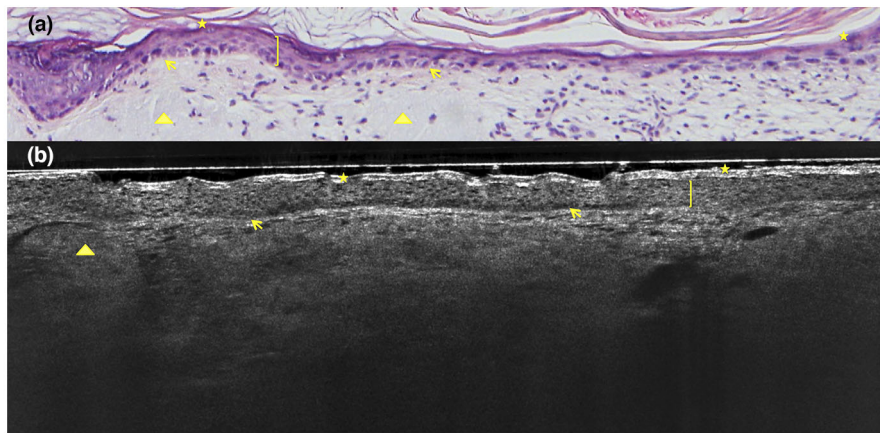
Figure 2 Atrophic AK of the face: H&E stained histology (100×) (a), LC-OCT in vertical mode (b) Note hyperkeratosis/parakeratosis (star), atypical keratinocytes (bracket) with preserved DEJ and flattened rete ridges (arrow), solar elastosis (triangle). AK, actinic keratosis; DEJ, dermo-epidermal junction; H&E, haematoxylin–eosin; LC-OCT, line-field confocal optical coherence tomography.

sun-damaged skin, AKs and SCCs based on the analysis of cellular, 3D microarchitectural structures and tissue scattering.[35]

In this article, we focused on LC-OCT features of AK, BD and SCC, in order to correlate the presence of specific descriptors with the stage of KC.

Hyperkeratosis was visible as a hyperreflective multilayer of polygonal cells with sometimes remaining nuclei (parakeratosis). Atypical keratinocytes were polygonal structures with a dark cytoplasm and bright contours, enlarged in comparison with those in healthy epidermis and with inhomogeneous size and shape. The cellular layering was intuitively comparable with the corresponding histological sections. However, it was not always easy to systematically differentiate basal and suprabasal keratinocyte atypia; to this regard, we noticed that the differences were easier detectable with higher grades of dysplasia (BD, SCC). Acantholysis was seen as darker spaces between the epidermal keratinocytes. Also, fragmented (pycnotic) keratinocytes could be detected.

The epidermal thickness systematically and significantly increased with the progression to invasive SCC.

In the dermis, increased vascularization and collagen fibre disarrangement, corresponding to elastosis (collagen reaction), were seen in all types of lesions in both vertical and horizontal sections. Small bright particles, probably corresponding to inflammatory infiltrates, could be visualized in both the epidermal and dermal layers.

We could visualize AKs and their main histopathological correlates with LC-OCT; the device also seemed to be potentially useful in AK subtyping. Although we only analysed a very small sample of AK subtypes (10 hypertrophic, 5 atrophic and 3 bowenoid), we were able to preliminarily observe the characteristic flattening of the rete in hypertrophic AKs, a thinned epidermis

in atrophic AKs and the typical full thickness keratinocyte dysplasia with roundish contours in bowenoid AKs. In early AKs, the dermoscopic structureless red areas interrupted by follicular openings were associated with dilated and tortuous hyporeflective vessels in the superficial dermis and hyperreflective, follicular hyperkeratosis. A larger, systematic study on AKs subtyping should be performed to further investigate this interesting topic.

In BD, the enlarged atypical keratinocytes built a thickened, acanthotic epidermis with roundish ('bowenoid') contours of the enlarged atypical keratinocytes in all epidermal layers, which we defined as bowenoid pattern. This was the main feature to distinguish BD from AKs and SCCs.

In BDs and AKs, the DEJ was well preserved, seen as a darker band separating the basal keratinocytes from the bright dermal collagen; however, in 7 AKs and 2 BD, some parts of the DEJ were not visible, due to the increased thickness of the stratum corneum, pointing towards the limited penetration depth of LC-OCT, which does not always allow a complete examination of the epidermis and DEJ in thick hyperkeratotic lesions. Possible strategies to partially overcome this limit may be, as in conventional OCT and RCM, focusing on the lesion borders and/or removing thick hyperkeratotic crusts, thus with the risk of bleeding and inflammation impeaching the examination.

Squamous cell carcinomas are invasive, keratinizing tumours, composed of large keratinocytes displaying different grades of atypia, arising from the epidermis and extending into the dermis. In LC-OCT, disarranged masses of large polygonal cells with irregular contours could be seen; roundish bright homogeneous structures corresponding to horn pearls were visible. When visible, the dermis was infiltrated by tumour strands and masses, with increased and irregular vascularization (dilated vessels/neoangiogenesis) and bright collagen bundles
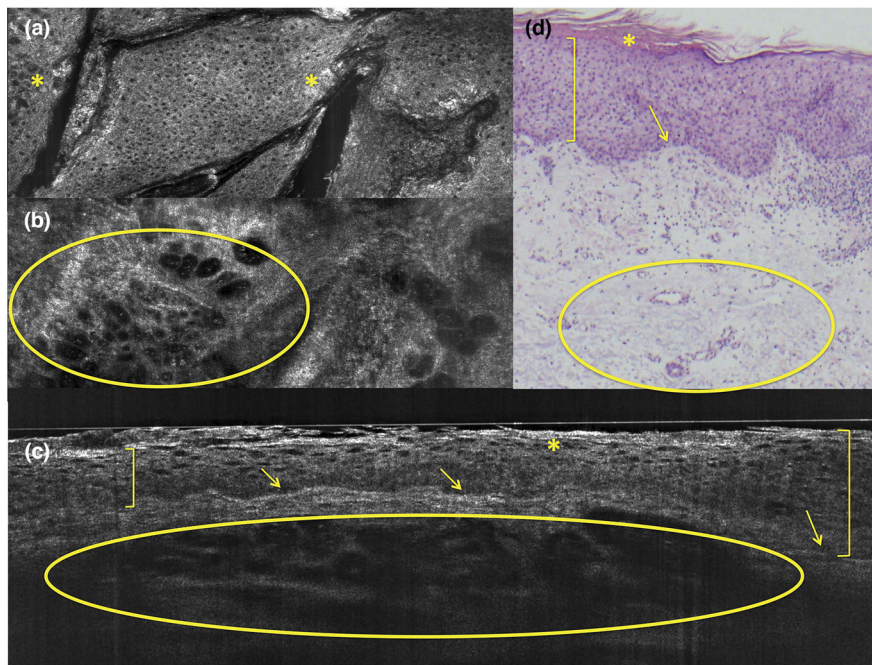
Figure 3 BD of the back: LC-OCT in horizontal mode at the epidermis (a) and junctional (b) level, vertical mode (c) and H&E stained histology (40×) (d). Atypical keratinocytes (bracket), hyperkeratosis with parakeratosis (asterisk), preserved DEJ (arrow), dilated vessels (circle) are seen. BD, Bowen disease; DEJ, dermo-epidermal junction; H&E, haematoxylin–eosin; LC-OCT, line-field confocal optical coherence tomography.

(elastosis/collagen alterations). In the descriptive statistics, these findings were more common in SCCs compared with AKs and BDs, although the model did not reach a statistical significance probably due to the small sample size.

If we take into account RCM, Peppelman and colleagues found architectural disarray in the stratum granulosum–spinosum and nest-like structures in the dermis as predictors of SCC compared to AK, based on 30 lesions.[29,36] Manfredini *et al.* listed erosion, architectural disarrangement and speckled nucleated cells in the dermis as the most common SCC features; buttonhole vessels were mostly found in in situ SCCs, while irregularly dilated vessels could be detected in invasive SCCs.[17] In horizontal LC-OCT images, which are intuitively comparable to RCM ones, we could describe an atypical honeycombed pattern constituted of dark polygonal cells in different sizes and shapes in all lesions; the grade of atypia increased from AK to SCC. Pyknotic cells were also visible. Collagen alterations/elastosis were seen, but we did not find any predominant vascular morphology.

A supplementary point was to evaluate whether specific LC-OCT descriptors were significantly associated with different stages of keratinocyte cancer. In fact, recognizing the invasiveness of the tumour is necessary for the therapeutic planning, since most AKs and BDs do not require a surgical approach. We therefore included all predictors that showed a significant odds ratio, in a multivariate multinomial logistic regression with bidirectional elimination based on previous studies about other diagnostic techniques,[29] and extrapolated dermoscopic and LC-OCT characteristics that can be useful in the correct classification of different subtypes of KC. In fact, a few patterns immediately help recognize different KC types. For example, a continuous DEJ is a typical feature of AK and BD, but cannot be seen in SCC, where an interrupted DEJ, marked collagen alterations and bright (inflammatory) particles in the dermis are prevalent. Even different types of AKs can be better recognized compared with dermoscopy: flattened rete ridges are typical for hypertrophic AKs, while a thinned epidermis was found in atrophic AKs. The model was conceived to calculate the correct classification rate of LC-OCT for AK, BD and SCC, which was 100%. However, due to overfitting, we based the interpretation of our results and discussion on the univariate multinomial logistic regressions. These results should be considered as preliminary and serve as a hint for future studies on larger samples, including more BD and SCCs compared with AKs.
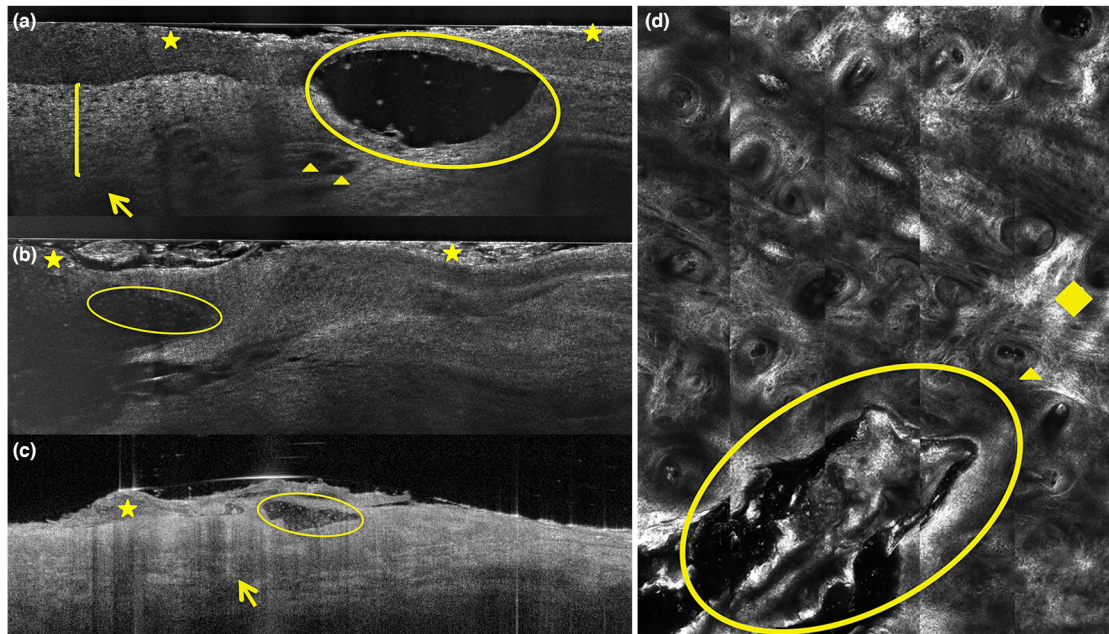
Figure 4 SCC of the scalp in vertical LC-OCT (a, b), OCT (c) and RCM (d). We see the following: a thick hyperkeratotic crust (asterisk), ulceration/blood crust (circle), atypical keratinocytes (bracket) with loss of the DEJ (arrow), dilated vessels (triangle), marked architectural disarrangement and elastosis (rhombus) also at the periphery of the lesion. DEJ, dermo-epidermal junction; H&E, haematoxylin–eosin; LC-OCT, line-field confocal optical coherence tomography; OCT, optical coherence tomography; RCM, reflectance confocal microscopy; SCC, squamous cell carcinoma.

Advantages and limitations of LC-OCT compared with other diagnostic techniques should be briefly discussed. The scanning camera allows the direct navigation of the examined area, as in conventional OCT and RCM 1500®. The unique combination of vertical and horizontal images at nearly cellular resolution makes histopathological correlations easier and reduces diagnostic pitfalls. The limited resolution compared with RCM does not impeach the evaluation of the keratinocyte atypia, but might complicate the differential diagnosis with melanocytic lesions. Offering less penetration depth than conventional OCT, LC-OCT can miss the deeper epidermal layers in the presence of massive hyperkeratosis, so that some thick early lesions might be misevaluated. Only conventional OCT offers a dynamic mode for blood flow.

Conclusions

We believe that the integration of clinical, dermoscopic and imaging data improves the therapeutic planning and follow-up of KC. In our experience, LC-OCT recognizes main features (keratinocyte morphology, architecture and DEJ structure) and allows the diagnosis of different stages of KC with intuitive and reliable histopathological correlations. Our findings open new scenarios in the non-invasive characterization of field cancerization. Further studies are needed to correlate the LC-OCT images to other histologic AK classifications such as PRO (a model focused on different stages of downward extension of basal keratinocytes 'protruding' into the papillary dermis)[37,38] and to standardize imaging algorithms for AKs, BD and SCCs.

References

1 Leiter U, Heppt MV, Steeb T *et al*. S3 guideline for actinic keratosis and cutaneous squamous cell carcinoma (cSCC) - short version, part 2: epidemiology, surgical and systemic treatment of cSCC, follow-up, prevention and occupational disease. *J Dtsch Dermatol Ges* 2020; **18**: 400–413.

2 Malvehy J. A new vision of actinic keratosis beyond visible clinical lesions. *J Eur Acad Dermatol Venereol* 2015; **29**(Suppl 1): 3–8.

3 Zalaudek I, Giacomel J, Schmid K *et al*. Dermatoscopy of facial actinic keratosis, intraepidermal carcinoma, and invasive squamous cell carcinoma: a progression model. *J Am Acad Dermatol* 2012; **66**: 589–597.

4 Rosendahl C, Cameron A, Argenziano G, Zalaudek I, Tschandl P, Kittler H. Dermoscopy of squamous cell carcinoma and keratoacanthoma. *Arch Dermatol* 2012; **148**: 1386–1392.

5 Dinnes J, Deeks JJ, Chuchu N *et al*. Visual inspection and dermoscopy, alone or in combination, for diagnosing keratinocyte skin cancers in adults. *Cochrane Database Syst Rev* 2018; **12**: Cd011901.

6 Witkowski A, Łudzik J, DeCarvalho N *et al.* Non-invasive diagnosis of pink basal cell carcinoma: how much can we rely on dermoscopy and reflectance confocal microscopy? *Skin Res Technol* 2016; **22**: 230–237.

7 Valdés-Morales KL, Peralta-Pedrero ML, Cruz FJ, Morales-Sánchez MA. Diagnostic accuracy of dermoscopy of actinic keratosis: a systematic review. *Dermatol Pract Concept* 2020; **10**: e2020121.

8 Zalaudek I, Kreusch J, Giacomel J, Ferrara G, Catricala C, Argenziano G. How to diagnose nonpigmented skin tumors: a review of vascular structures seen with dermoscopy: part I. Melanocytic skin tumors. *J Am Acad Dermatol* 2010; **63**: 361–374.

9 Reinehr CP, Garbin GC, Bakos RM. Dermatoscopic patterns of nonfacial actinic keratosis: characterization of pigmented and nonpigmented lesions. *Dermatol Surg* 2017; **43**: 1385–1391.

10 Huerta-Brogeras M, Olmos O, Borbujo J *et al.* Validation of dermoscopy as a real-time noninvasive diagnostic imaging technique for actinic keratosis. *Arch Dermatol* 2012; **148**: 1159–1164.

11 Navarrete-Dechent C, Bajaj S, Marchetti MA, Rabinovitz H, Dusza SW, Marghoob AA. Association of shiny white blotches and strands with nonpigmented basal cell carcinoma: evaluation of an additional dermoscopic diagnostic criterion. *JAMA Dermatol* 2016; **152**: 546–552.

12 Ruini C, Hartmann D, Bastian M *et al.* Non-invasive monitoring of subclinical and clinical actinic keratosis of face and scalp under topical treatment with ingenol mebutate gel 150 mcg/g by means of reflectance confocal microscopy and optical coherence tomography: New perspectives and comparison of diagnostic techniques. *J Biophotonics* 2019; **12**: e201800391.

13 Ulrich M, Krueger-Corcoran D, Roewert-Huber J, Sterry W, Stockfleth E, Astner S. Reflectance confocal microscopy for noninvasive monitoring of therapy and detection of subclinical actinic keratoses. *Dermatology* 2010; **220**: 15–24.

14 Themstrup L, Pellacani G, Welzel J, Holmes J, Jemec GBE, Ulrich M. In vivo microvascular imaging of cutaneous actinic keratosis, Bowen's disease and squamous cell carcinoma using dynamic optical coherence tomography. *J Eur Acad Dermatol Venereol* 2017; **31**: 1655–1662.

15 Dejonckheere G, Suppa M, Del Marmol V, Meyer T, Stockfleth E. The actinic dysplasia syndrome - diagnostic approaches defining a new concept in field carcinogenesis with multiple cSCC. *J Eur Acad Dermatol Venereol* 2019; **33**(Suppl 8): 16–20.

16 Guida S, Longo C, Casari A *et al.* Update on the use of confocal microscopy in melanoma and non-melanoma skin cancer. *G Ital Dermatol Venereol* 2015; **150**: 547–563.

17 Manfredini M, Longo C, Ferrari B *et al.* Dermoscopic and reflectance confocal microscopy features of cutaneous squamous cell carcinoma. *J Eur Acad Dermatol Venereol* 2017; **31**: 1828–1833.

18 Navarrete-Dechent C, DeRosa AP, Longo C *et al.* Reflectance confocal microscopy terminology glossary for nonmelanocytic skin lesions: A systematic review. *J Am Acad Dermatol* 2019; **80**: 1414–1427.e3.

19 Friis KBE, Themstrup L, Jemec GBE. Optical coherence tomography in the diagnosis of actinic keratosis-A systematic review. *Photodiagnosis Photodyn Ther* 2017; **18**: 98–104.

20 Ruini C, Schuh S, Sattler E, Welzel J. Line-field confocal optical coherence tomography—Practical applications in dermatology and comparison with established imaging methods. *Skin Res Technol* 2021; **27**: 340–352. http://dx.doi.org/10.1111/srt.12949.

21 Ruini C, Sattler E. Konfokale Line-Field-OCT: die eierlegende Wollmilchsau?. *Aktuelle Dermatol* 2020; **46**: 148–151. http://dx.doi.org/10.1055/a-1072-7002.

22 Tognetti L, Fiorani D, Suppa M *et al.* Examination of circumscribed palmar hypokeratosis with line-field confocal optical coherence tomography: Dermoscopic, ultrasonographic and histopathologic correlates. *Indian J Dermatol Venereol Leprol* 2020; **86**: 206–208.

23 Monnier J, Tognetti L, Miyamoto M *et al.* In vivo characterization of healthy human skin with a novel, non-invasive imaging technique: line-field confocal optical coherence tomography. *J Eur Acad Dermatol Venereol* 2020; **34**: 2914–2921. http://dx.doi.org/10.1111/jdv.16857.

24 Dubois A, Levecq O, Azimani H *et al.* Line-field confocal optical coherence tomography for high-resolution noninvasive imaging of skin tumors. *J Biomed Opt* 2018; **23**: 1–9.

25 Ruini C, Schuh S, Hartmann D, French L, Welzel J, Sattler E. Noninvasive real-time imaging of mite skin infestations with line-field confocal optical coherence tomography. *Br J Dermatol* 2020; **184**.

26 Ogien J, Daures A, Cazalas M, Perrot J-L, Dubois A. Line-field confocal optical coherence tomography for three-dimensional skin imaging. *Front Optoelectron* 2020; **13**: 381–392. http://dx.doi.org/10.1007/s12200-020-1096-x.

27 Dubois A, Levecq O, Azimani H *et al.* Line-field confocal time-domain optical coherence tomography with dynamic focusing. *Opt Express* 2018; **26**: 33534–33542.

28 Ogien J, Levecq O, Azimani H, Dubois A. Dual-mode line-field confocal optical coherence tomography for ultrahigh-resolution vertical and horizontal section imaging of human skin. *Biomed Opt Express* 2020; **11**: 1327–1335.

29 Peppelman M, Nguyen KP, Hoogedoorn L, van Erp PE, Gerritsen MJ. Reflectance confocal microscopy: non-invasive distinction between actinic keratosis and squamous cell carcinoma. *J Eur Acad Dermatol Venereol* 2015; **29**: 1302–1309.

30 Olsen J, Themstrup L, De Carvalho N, Mogensen M, Pellacani G, Jemec GB. Diagnostic accuracy of optical coherence tomography in actinic keratosis and basal cell carcinoma. *Photodiagnosis Photodyn Ther* 2016; **16**: 44–49.

31 Ulrich M, Themstrup L, de Carvalho N *et al.* Dynamic optical coherence tomography of skin blood vessels - proposed terminology and practical guidelines. *J Eur Acad Dermatol Venereol* 2018; **32**: 152–155.

32 Ferrante di Ruffano L, Dinnes J, Deeks JJ *et al.* Optical coherence tomography for diagnosing skin cancer in adults. *Cochrane Database Syst Rev* 2018; **12**: Cd013189.

33 Schuh S, Kaestle R, Sattler EC, Welzel J. Optical coherence tomography of actinic keratoses and basal cell carcinomas - differentiation by quantification of signal intensity and layer thickness. *J Eur Acad Dermatol Venereol* 2016; **30**: 1321–1326.

34 Batz S, Wahrlich C, Alawi A, Ulrich M, Lademann J. Differentiation of different nonmelanoma skin cancer types using OCT. *Skin Pharmacol Physiol* 2018; **31**: 238–245.

35 Boone MA, Suppa M, Marneffe A, Miyamoto M, Jemec GB, Del Marmol V. A new algorithm for the discrimination of actinic keratosis from normal skin and squamous cell carcinoma based on in vivo analysis of optical properties by high-definition optical coherence tomography. *J Eur Acad Dermatol Venereol* 2016; **30**: 1714–1725.

36 Nguyen KP, Peppelman M, Hoogedoorn L, Van Erp PE, Gerritsen MP. The current role of in vivo reflectance confocal microscopy within the continuum of actinic keratosis and squamous cell carcinoma: a systematic review. *Eur J Dermatol* 2016; **26**: 549–565.

37 Schmitz L, Gupta G, Stücker M *et al.* Evaluation of two histological classifications for actinic keratoses - PRO classification scored highest inter-rater reliability. *J Eur Acad Dermatol Venereol* 2019; **33**: 1092–1097.

38 Schmitz L, Gambichler T, Gupta G *et al.* Actinic keratoses show variable histological basal growth patterns - a proposed classification adjustment. *J Eur Acad Dermatol Venereol* 2018; **32**: 745–751.

Supporting information

Additional Supporting Information may be found in the online version of this article:

Figure S1. Hypertrophic AK of the scalp: in vertical LC-OCT (a) and H&E stained histology (40×): hyperkeratosis/parakeratosis (star) together with atypical keratinocytes (bracket) are seen, while the DEJ is preserved (arrow); solar elastosis is present (triangle).

Figure S2. Detail of the cellular morphology of a clear cell BD in LC-OCT in horizontal mode (a) and H&E stained histology (100×) (b). Hyperkeratosis with parakeratosis (star) and large atypical keratinocytes (bracket) are seen.

Table S1. Descriptive statistics of dermoscopic features of actinic keratosis, Bowen's disease, and squamous cell carci-noma evaluated in the study with their relative and absolute frequencies.

Table S2. Univariate multinomial logistic regression reporting odds ratios (OR) and *P*-values of main analysed dermoscopic patterns.